American Mineralogist, Volume 85, pages 745–752, 2000

Two proton positions in the very strong hydrogen bond of serandite, $NaMn_2[Si_3O_8(OH)]$

STEVEN D. JACOBSEN,[1,2,*] JOSEPH R. SMYTH,[1,2] R. JEFFREY SWOPE,[1] AND ROBERT I. SHELDON[3]

[1]Department of Geological Sciences, University of Colorado, Boulder, Colorado 80309-0399, U.S.A.
[2]Bayerisches Geoinstitut, Universität Bayreuth, D-95440 Bayreuth, Germany
[3]Los Alamos National Laboratory, Los Alamos, New Mexico, 87545, U.S.A.

ABSTRACT

The crystal structure and hydrogen positions of serandite, $NaMn_2[Si_3O_8(OH)]$, have been refined from single-crystal X-ray and time-of-flight neutron diffraction data at ambient conditions. The proton occupies an asymmetric, double-well position between O3 and O4, confirming one of the shortest asymmetric hydrogen bonds known in minerals with d(O3…O4) = 2.464(1) Å (X-ray) and 2.467(1) Å (neutron). The proton position closest to O3 has about 84% occupancy and an O-H distance of 1.078(3) Å, and the position closest to O4 has an occupancy of 16% and an O-H distance of 1.07(1) Å. The d(H…O) of these hydrogen bonds is 1.413(3) Å and 1.41(1) Å, respectively. Hydrogen bond angles are 164° for H1 and 168° for H2. The Si^{IV}-OH bond length [1.628(1) Å] is intermediate in length among the three other Si-O bonds in the dominantly (84%) hydrated Si1 tetrahedron. These new structure data for a very strong hydrogen bond may be useful for extending spectroscopy-structure correlation diagrams into the region of very low energy O-H stretching.

INTRODUCTION

Hydrogen occurs in nearly all rock-forming minerals in major, minor, or trace amounts. Protonation of non-silicate oxygen positions is by far the most common mechanism of hydration of silicates by hydroxyl (OH^-). The isostructural pyroxenoids, serandite $NaMn_2[Si_3O_8(OH)]$, and pectolite $NaCa_2[Si_3O_8(OH)]$, however, contain stoichiometric hydrogen as hydroxyl bound to a non-bridging silicate oxygen in the chain. The resulting Si^{IV}-OH bond provides the unique opportunity to study the geometry of a silanol group associated with a very strong (short) hydrogen bond.

The nature of Si-OH bonding is relatively unknown compared to the ubiquitous Si-O bond (Pauling 1980). Nyfeler and Armbruster (1998) searched the Inorganic Crystal Structure Database (Bergerhoff et al. 1983) for silanol groups and found 31 inorganic compounds with 46 Si-OH groups. They restricted their search to compounds and minerals in which the distance from Si to H was less than 2.8 Å, and they excluded structures with disordered or poorly defined hydrogen positions. Serandite and pectolite were not included in their investigation because the proton position was not unambiguously known from the available X-ray structure refinements of pectolite (Prewitt 1967; Takéuchi and Kudoh 1977) and serandite (Takéuchi et al. 1976).

Buerger (1956) solved the main aspects of the pectolite structure using film methods. The structure was refined in space group $P\bar{1}$ by Prewitt and Buerger (1963), who first proposed that a hydrogen bond most likely exists between the very close (2.48 Å), non-bridging oxygen pair, O3 and O4, along the chain. They applied Pauling's valence sum at O3 and O4 and found that both sites are equally underbonded by about 0.5 valence units. Prewitt (1967) further refined the pectolite structure from digital X-ray diffraction data, and identified a small residual peak between O3 and O4 in the electron density difference-Fourier. Although the residual was not significantly above the background, it had a clear maximum about 0.97 Å from O3, and spread out smoothly towards O4. Prewitt (1967) proposed that an asymmetric hydrogen bond might form with O3-H…O4, but that it would be highly unusual for such a short hydrogen bond distance.

Takéuchi et al. (1976) refined the structure of serandite and found that the O3…O4 distance was about 2.453(4) Å, significantly shorter than in pectolite. They also observed a residual charge density between O3 and O4, but found that the peak was about 1.25 Å from both oxygen positions, resulting in a more symmetrical hydrogen bond than proposed by Prewitt (1967) for pectolite. Although Takéuchi et al. (1976) were unable to uniquely determine the hydrogen position, they postulated an alternate mode of hydrogen bonding in which H would form a hydrogen bond between O3 and the O3' of an adjacent silicate chain. Subsequently, Takéuchi and Kudoh (1977) studied a manganoan pectolite crystal by X-ray diffraction with the intention of resolving the (X-ray) hydrogen position. They found that, in agreement with Prewitt (1967), the difference-Fourier peak in the electron density from H was closer to O3, but also very broad. On the shoulder of this broad peak and closer to O4, they defined a second H position, H2. From this model, they proposed a disordered mode of H bonding along the chain that would alternate between O3-H…O4 and O3…H-O4 configurations.

Structural interpretation of infrared absorption spectra of hydrogen bonds from frequency-distance correlations in organic compounds (Lutz 1995; Mikenda 1986; Nakamoto et al. 1955;

*E-mail: steven.jacobsen@colorado.edu

Novak 1974) and minerals (Libowitzky 1999) requires the precise location of H from experiment. Hammer et al. (1998) measured polarized infrared absorption spectra of single-crystal pectolite and serandite in which they observe a very broad absorption band parallel to *b* and centered around 1000 cm^{-1}, to which they assign the fundamental O-H stretching vibration. Hydrogen bonds which display O-H stretching at frequencies below 1600 cm^{-1} are considered to be very strong (Emsley 1981). Hammer et al. (1998) also observed, parallel to *c*, a bending mode at about 1396 cm^{-1} in pectolite and 1386 cm^{-1} in serandite, which suggests that the hydrogen bond in pectolite is slightly stronger relative to serandite. The IR results indicate an extremely low energy of the O-H stretching vibration, consistent with a very strong hydrogen bond between O3 and O4. Based on comparison to other structures with very strong hydrogen bonds, such as natrochalcite-type compounds (Beran et al. 1997), Hammer et al. (1998) conclude that the spectroscopy results support an asymmetric O-H…O bond in serandite-pectolite, though structure data from neutron diffraction were not available for comparison.

Hydrogen bond geometry is also known to have strong isotopic fractionation effects (Novak 1974). Short, strong hydrogen bonds with short O…O distances are likely to preferentially concentrate lighter isotopes of hydrogen. Indeed, Kuroda et al. (1979) found that pectolite has one of the lowest δD values (about –400‰) of any previously measured silicate, with the exception of rocks returned from the surface of the moon. This is also consistent with the unusually low energy of the O-H stretching vibration and relatively long O-H distance. A future investigation of the correlation between hydrogen isotope fractionation and hydrogen bond geometry will require precise H positions from neutron diffraction.

To resolve questions of the relation of H bonding geometry to IR spectroscopy, we refined the structure of serandite using data from both rotating anode X-ray and time-of-flight neutron diffraction. Our principal objectives are to define the H position with sufficient precision to decide whether there is a single (ordered) or double (disordered) position and, if possible, to determine the hydrogen bond O…O, O-H, and H…O distances to high precision. This should allow a better understanding of the controls of H bonding geometry on the IR spectra of this highly unusual type of hydrogen bond.

Experimental procedure

Large, centimeter-sized single crystals of serandite from Mont Saint Hilaire, Quebec, were provided by Pete J. Dunn at the Smithsonian National Museum of Natural History. The X-ray sample (NMNH no. 132508) and the neutron sample (NMNH no. 137493) are nearly end-member specimens with approximate chemistry: $(Mn_{2.00}Ca_{0.03})NaHSi_3O_9$, including H_2O by difference, determined by electron microprobe analysis.

X-ray diffraction

For the X-ray experiment, a cleavage fragment measuring approximately 180 μm × 120 μm × 150 μm was chosen from the bulk material. The crystal was mounted and optically centered on a Siemens, P4 four-circle diffractometer equipped with a Mo rotating anode target and 18 kW generator operating at 50 kV and 250 mA. The instrument is also fitted with an incident beam graphite monochromator. Unit-cell parameters were determined from the centered positions of 25 unique reflections, measured in both positive and negative 2θ to eliminate zero-point errors. Results are listed in Table 1.

Intensity data were collected using variable speed, θ-2θ scan mode with 2θ speeds ranging from 4 to 40 °/min to allow for adequate counting statistics. A doubly redundant (centric) sphere of data were collected from 2θ = 2 to 80° resulting in 8972 reflections, of which 4232 are unique with $I > 2\sigma(I)$. Three standard reflections were measured every 100 reflections to monitor the instrument stability over the relatively long (6 day) data collection. The data were corrected for Lorentz and polarization effects. The average I/σ for this data set is 48. The data were corrected for absorption ($\mu = 4.21/\mu m$) using an analytical absorption correction routine (Sheldrick 1990) which uses the measured dimensions and indexed faces of the crystal with direction cosines of each reflection to calculate the X-ray path length through the crystal. The atom positions and displacement parameters were refined using SHELXTL (Sheldrick 1990). Initial atom position parameters were those of Takéuchi et al. (1976), and scattering factors were those of neutral atoms. A small residual was observed between the O3 and O4 and a neutral H atom with a large isotropic displacement parameter was placed at this position. The position and displacement parameters were then refined. The final model converged to an $R(F) = 0.020$ for the 4232 unique reflections with $I > 2\sigma(I)$. Atom positions from the final model for serandite from the X-ray study are reported in Table 2. Anisotropic (U_{ij}) and isotropic equivalent (U_{eq}) displacement parameters are given in Table 3. Interatomic distances and polyhedral volumes, occupancies, and distortion parameters are listed in Tables 4 and 5.

A single hydrogen position in the X-ray model was obtained at $x/a = 0.179(4)$, $y/b = 0.621(4)$, and $z/c = 0.533(4)$, with a rather large isotropic displacement parameter, $U_{eq} = 0.064(7)$ Å^2. This position corresponds to the configuration O3-H…O4. The O-H distance of this position is 0.94(3) Å, which is short, but consistent with O-H distances determined from X-ray diffraction. The hydrogen bond distance is d(O…O) = 2.464(1) Å with d(H…O) = 1.53(3) Å, and a hydrogen bond angle of 174(3)°. Although the reported hydrogen bond geometry in serandite from this study will come from the neutron results, the X-ray hydrogen position may be useful to future studies that compare H positions derived from X-ray vs. neutron diffraction experiments (Finney 1995).

To check for minor Ca substitution for Mn (Ohashi 1976; Ohashi and Finger 1978), we refined the site occupancy of the

Table 1. Unit-cell parameters for the serandite samples (space group $P\bar{1}$), determined from X-ray and neutron diffraction

Serandite sample	X-ray NMNH no.132508	Neutron NMNH no.137493
a (Å)	7.7185(4)	7.7163(7)
b (Å)	6.9064(5)	6.9116(7)
c (Å)	6.7624(5)	6.7368(5)
α (°)	90.492(5)	90.465(7)
β (°)	94.085(5)	94.037(7)
γ (°)	102.775(6)	102.844(7)
V (Å^3)	350.56(5)	349.32(5)
ρ_{calc} (g/cm^3)	3.431	3.403

TABLE 2. Fractional coordinates and occupancy parameters for serandite

Atom	*x*/*a*	*y*/*b*	*z*/*c*	occ.	elec. pot. (V)
Na	0.55614(5)	0.25385(7)	0.35237(7)	1.0	–12.39
	0.5557(2)	0.2553(3)	0.3529(3)		
Mn1	0.85219(2)	0.59405(2)	0.13637(2)	0.944(1)	–23.78
	0.8531(2)	0.5945(2)	0.1349(3)	0.941(9)	
Mn2	0.84956(2)	0.08396(2)	0.13308(2)	0.989(1)	–22.85
	0.8491(2)	0.0840(2)	0.1329(2)	0.983(9)	
Si1	0.21589(3)	0.40239(3)	0.34113(3)	1.0	–47.93
	0.2151(2)	0.4017(2)	0.3424(2)		
Si2	0.20581(3)	0.95249(3)	0.35090(3)	1.0	–46.69
	0.2059(2)	0.9511(2)	0.3512(2)		
Si3	0.45398(3)	0.73904(3)	0.14312(3)	1.0	–44.97
	0.4543(2)	0.7370(2)	0.1428(2)		
O1	0.66327(8)	0.79612(10)	0.11507(10)	1.0	27.62
	0.6643(1)	0.7943(1)	0.1138(2)		
O2	0.32289(9)	0.70965(10)	0.94371(9)	1.0	27.36
	0.3226(1)	0.7065(1)	0.9435(2)		
O3	0.18070(9)	0.49542(10)	0.55276(10)	1.0	21.21
	0.1788(1)	0.4926(1)	0.5554(2)		
O4	0.15867(9)	0.84596(9)	0.55620(9)	1.0	23.46
	0.1598(1)	0.8443(1)	0.5572(2)		
O5	0.06121(8)	0.39059(10)	0.16778(9)	1.0	25.60
	0.0614(1)	0.3912(1)	0.1671(2)		
O6	0.05273(8)	0.89324(10)	0.17232(9)	1.0	27.46
	0.0519(1)	0.8912(1)	0.1724(2)		
O7	0.40696(8)	0.53359(9)	0.27366(10)	1.0	32.11
	0.4071(1)	0.5335(1)	0.2772(2)		
O8	0.39617(8)	0.90570(9)	0.28860(10)	1.0	32.59
	0.3972(1)	0.9067(1)	0.2866(2)		
O9	0.26035(8)	0.19025(9)	0.39346(10)	1.0	32.46
	0.2593(1)	0.1888(1)	0.3931(2)		
H_{xray}	0.179(4)	0.621(4)	0.533(4)	1.0	
H1	0.1482(4)	0.6374(4)	0.5498(5)	0.842(6)	
H2	0.1518(17)	0.6872(16)	0.5483(22)	0.158(6)	

Note: First row (X-ray) and second row (neutron) structure refinements. Electrostatic site potentials are calculated with no hydrogen in the model. In the neutron model, the sum of the occupancies of H1 and H2 were constrained to equal 1.0, and were not refined during the final cycles of least-squares.

TABLE 3. Thermal displacement parameters (×100) for serandite

Atom	U_{11}	U_{22}	U_{33}	U_{12}	U_{13}	U_{23}	U_{eq}
Na	0.87(2)	1.78(2)	1.67(2)	0.13(1)	0.24(1)	0.01(2)	1.46(1)
	0.80(6)	1.49(7)	1.95(9)	0.00(5)	0.28(6)	0.05(6)	1.45(6)
Mn1	0.817(6)	0.719(5)	0.775(6)	0.144(4)	0.110(4)	0.019(4)	0.772(3)
	0.76(6)	0.70(6)	0.91(7)	0.03(4)	0.07(5)	0.02(5)	0.81(6)
Mn2	0.780(6)	0.814(5)	0.777(5)	0.251(4)	0.076(4)	–0.010(4)	0.778(3)
	0.70(6)	0.69(6)	0.87(7)	0.21(4)	0.11(5)	–0.02(5)	0.74(6)
Si1	0.604(8)	0.492(8)	0.677(9)	0.151(6)	–0.037(6)	0.005(6)	0.590(5)
	0.46(4)	0.42(4)	0.73(5)	0.12(3)	0.07(4)	–0.01(4)	0.53(4)
Si2	0.621(8)	0.479(8)	0.601(8)	0.157(6)	–0.006(6)	–0.021(6)	0.564(5)
	0.54(4)	0.42(4)	0.53(5)	0.12(3)	0.04(4)	0.05(4)	0.49(4)
Si3	0.481(8)	0.619(8)	0.611(8)	0.109(6)	0.053(6)	–0.003(6)	0.572(5)
	0.40(4)	0.41(4)	0.69(5)	0.10(3)	0.02(4)	–0.05(4)	0.50(4)
O1	0.54(2)	1.12(2)	1.23(3)	0.05(2)	0.22(2)	0.00(2)	0.98(1)
	0.49(3)	0.75(4)	1.36(5)	0.08(3)	0.30(3)	0.008(3)	0.87(3)
O2	0.91(2)	1.24(2)	0.75(2)	0.29(2)	–0.15(2)	–0.06(2)	0.97(1)
	0.75(3)	0.87(4)	0.92(4)	0.16(3)	–0.15(3)	–0.07(3)	0.86(3)
O3	1.27(3)	0.99(2)	0.86(2)	0.53(2)	0.02(2)	–0.23(2)	1.00(1)
	1.05(4)	0.72(3)	0.84(4)	0.35(3)	0.10(3)	–0.14(3)	0.84(3)
O4	1.47(3)	0.74(2)	0.73(2)	0.22(2)	0.21(2)	0.13(2)	0.98(1)
	1.32(4)	0.56(3)	0.75(4)	0.14(3)	0.24(3)	0.15(3)	0.87(4)
O5	0.74(2)	1.17(2)	0.76(2)	0.18(2)	–0.12(2)	0.08(2)	0.90(1)
	0.63(3)	0.99(4)	0.71(4)	0.13(3)	–0.01(3)	0.10(3)	0.79(3)
O6	0.74(2)	1.03(2)	0.76(2)	0.19(2)	–0.12(2)	–0.12(2)	0.85(1)
	0.65(3)	0.77(4)	0.89(4)	0.12(3)	–0.11(3)	–0.07(3)	0.78(3)
O7	0.75(2)	0.85(2)	1.47(3)	0.06(2)	0.12(2)	0.42(2)	1.04(1)
	0.56(3)	0.72(3)	1.45(5)	0.01(3)	0.05(3)	0.42(3)	0.93(3)
O8	0.79(2)	1.01(2)	1.17(2)	0.39(2)	0.04(2)	–0.37(2)	0.97(1)
	0.64(3)	0.83(4)	1.33(5)	0.30(3)	0.05(3)	–0.41(3)	0.92(3)
O9	1.02(2)	0.48(2)	1.21(2)	0.23(2)	0.00(2)	0.03(2)	0.89(1)
	0.92(4)	0.32(3)	1.38(5)	0.18(3)	0.05(3)	–0.01(3)	0.86(3)
H_{xray}							6.4(7)
H1	2.04(10)	2.17(11)	2.11(12)	0.70(8)	0.37(9)	0.09(9)	2.06(10)
H2							1.5(2)

Note: First row (X-ray) and second row (neutron) structure refinements. In the neutron model, displacement parameters for H1 and H2 were not refined during the final cycles of least-squares.

TABLE 4. Polyhedral bond lengths and angles from the X-ray structure refinement of serandite

Central atom			Bond length (Å)	Bond angle (°)
Si1	O3*		1.628(1)	
	O5		1.601(1)	
	O7		1.648(1)	
	O9		1.614(1)	
	average		1.623	
	O3	O5	2.735(1)	115.8(1)†
	O3	O7	2.637(1)	107.2(1)
	O3	O9	2.571(1)	104.9(1)
	O5	O7	2.676(1)	110.9(1)
	O5	O9	2.692(1)	113.8(1)
	O7	O9	2.557(1)	103.2(1)
	average		2.645	109.3†
Si2	O4*		1.604(1)	
	O6		1.611(1)	
	O8		1.654(1)	
	O9		1.620(1)	
	average		1.622	
	O4	O6	2.710(1)	114.9(1)‡
	O4	O8	2.637(1)	108.1(1)
	O4	O9	2.612(1)	108.2(1)
	O6	O8	2.693(1)	111.1(1)
	O6	O9	2.677(1)	111.8(1)
	O8	O9	2.541(1)	101.8(1)
	average		2.645	109.3‡
Si3	O1		1.601(1)	
	O2		1.610(1)	
	O7		1.662(1)	
	O8		1.662(1)	
	average		1.634	
	O1	O2	2.732(1)	116.5(1)§
		O7	2.665(1)	109.4(1)
		O8	2.687(1)	110.8(1)
	O2	O7	2.659(1)	108.6(1)
		O8	2.648(1)	108.0(1)
	O7	O8	2.591(1)	102.4(1)
	average		2.664	109.3§
Mn1	O1		2.229(1)	
	O2		2.267(1)	
	O3		2.212(1)	
	O5		2.363(1)	
	O5'		2.204(1)	
	O6		2.291(1)	
	average		2.261	
Mn1 site number of electrons			23.610(1)e⁻	
Mn2	O1		2.177(1)	
	O2		2.197(1)	
	O4		2.161(1)	
	O5		2.370(1)	
	O6		2.264(1)	
	O6'		2.244(1)	
	average		2.236	
Mn2 site number of electrons			24.735(1) e⁻	
Na	O2		2.262(1)	
	O3		2.403(1)	
	O4		2.487(1)	
	O7		2.501(1)	
	O7		2.878(1)	
	O8		2.467(1)	
	O8		2.710(1)	
	O9		2.265(1)	
	average		2.497	

*Si-OH group.
†O-Si1-O angle.
‡O-Si2-O angle.
§O-Si3-O angle.

octahedral Mn1 and Mn2 positions. We converted to the scale of number of electrons by modeling the site with 100% Mn and then multiplying the fractional occupancy by 25 e^- (Table 4). The Mn1 and Mn2 sites require 23.6 and 24.7 electrons, respectively, to best match the intensity data. There are fewer electrons at Mn1, which implies that Ca in the structure preferentially occupies the Mn1 site. This is consistent with the results of Takéuchi et al. (1977) who refined an intermediate composition serandite with approximate chemistry, $Na(Mn_{1.88}Ca_{0.17}Mg_{0.01})_2[Si_3O_8(OH)]$. This is also consistent with the fact that the Mn1 site is constrained to be slightly larger than the Mn2 site by its connection to the relatively rigid silicate chain.

Finally, to compare the electrostatic environment at the O3 and O4 positions, we calculated electrostatic site potentials for all the atoms in the structure, but with no H in the model (Table 2). We used a simple, nominal valence point-charge method described by Smyth (1989). Oxygen site potentials can be useful predictors of oxygen isotope fractionation (Smyth and Clayton 1988) and sites of protonation (Smyth 1987). In minerals, oxygen site-potential values of 28–30 V are typical for most silicate-oxygen positions of silicate tetrahedra. For serandite without H, the calculated electrostatic potentials at O3 and O4 are 21.2 and 23.5 V, respectively. Thus, both O3 and O4 are underbonded. The slightly shallower potential for O3 is more favorable for protonation over O4, consistent with the X-ray derived H position that is closer to O3.

Neutron diffraction

An elongated blade (1 cm) of peach-colored serandite NMNH no. 137493 was set in epoxy, and from this, an equant cube measuring about 2 mm per side was cut using a low-speed diamond saw. Long-exposure precession photographs of the oriented crystal reveal no significant mineral inclusions, mosaic structure, or damage from the cutting process. The crystal was taken to the Manuel Lujan Neutron Scattering Center (LANSCE) at the Los Alamos National Laboratory. The LANSCE facility uses a pulsed spallation neutron source for single-crystal and powder diffraction experiments. Intensity data are measured by a time- and position-sensitive area detector (20 $\times$ 20 cm) similar to that described by Borkowski and Kopp (1978). The detector records the position and time-of-flight (TOF) for each neutron, from which the energy (wavelength) can be calculated, given the instrument flight path distance. For serandite, 39 histograms of data were recorded to include the unique, $P\bar{1}$ triclinic hemisphere of reciprocal space. This resulted in 5287 total reflections, of which 4628 have $I > 3\sigma(I)$. Unit-cell parameters for this are listed in Table 1. The intensity data were corrected for background radiation, dead time, and then reduced to create a list of observed, integrated intensities. Each of the 39 histograms was adjusted to a common scale using the absolute count rate in an incident-beam ^{235}U fission monitor. Although the linear absorption coefficient for serandite is low, about 0.90/mm for 1.08 Å neutrons, we corrected the intensity data for absorption using the empirical, single-crystal absorption correction routine SCABS (Larson and Von Dreele 1994).

Using initial atom positions from our X-ray experiment, position and anisotropic displacement parameters were refined using

TABLE 5. Distortion parameters for serandite from the X-ray structure refinement

	Si1 tetrahedra	Si2 tetrahedra	Si3 tetrahedra	Mn1 octahedra	Mn2 octahedra	Na polyhedra
Polyhedral vol. (Å^3)	2.174	2.176	2.224	14.806	14.356	25.418
*Angle variance (deg^2)	25.14	20.13	20.96	95.33	84.28	
†Elongation	1.0059	1.0049	1.0048	1.0276	1.0258	

* Tetrahedral angle variance: $\sigma^2_{\theta(\text{tet})} = \sum_{i=1}^{6}\left(\theta_i - 109.47^\circ\right)/5$ (Robinson et al. 1971).

Octahedral angle variance: $\sigma^2_{\theta(\text{oct})} = \sum_{i=1}^{12}\left(\theta_i - 90^\circ\right)^2/11$.

† Tetrahedral quadratic elongation: $\langle\lambda_{\text{tet}}\rangle = \sum_{i=1}^{4}\left(l_i/l_o\right)^2/4$.

Octahedral quadratic elongation: $\langle\lambda_{\text{oct}}\rangle = \sum_{i=1}^{6}\left(l_i/l_o\right)^2/6$.

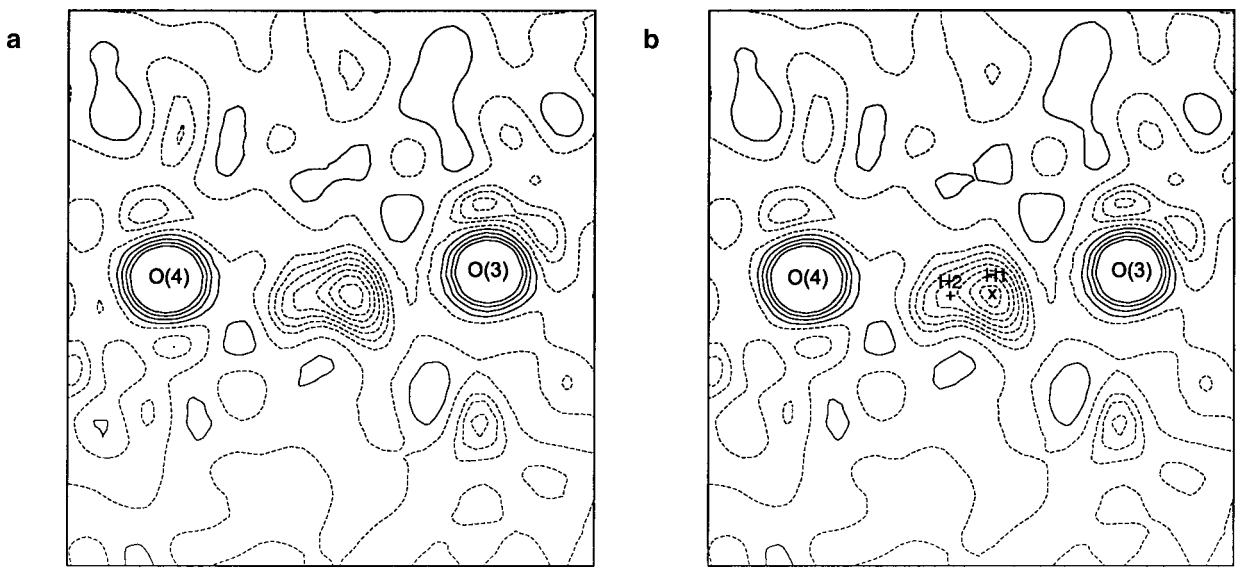

FIGURE 1. (**a**) Map of the observed scattering density F_{obs}. from the neutron diffraction study of serandite and (**b**) the calculated scattering density for the two-proton model. The model positions H1 and H2 are indicated by (x) and (+), respectively. In both maps, the section contains the hydrogen bond, O3, O4, and the *b*-axis, which is horizontal. Each map is 4 Å per side and contours are drawn at –2.0, –1.75, –1.5, –1.25, –1.0, –0.75, –0.5, 0, 0.5, 1.0, 1.5, and 2.0. The zero and negative contours are dashed.

the GSAS structure refinement package (Larson and Von Dreele 1994). We also refined a single, secondary extinction parameter of type II, described by Becker and Coppens (1974). The resulting extinction coefficient is $1.14(2)\times10^{-5}$. The initial model converged to an $R(F^2) = 0.102$ using all of the data, and $R(F^2) = 0.100$ or $R(F) = 0.063$ for the set of reflections with $I > 3\sigma(I)$. In this initial "one-proton" model, we refine a single H position between the O3 and O4 positions, corresponding to the H position that was refined in the X-ray model, O3-H…O4. The H position is well defined at $x/a = 0.1488(3)$, $y/b = 0.6438(4)$, and $z/c = 0.5497(3)$ and clearly closer to O3, forming an asymmetric hydrogen bond between O3 and O4. The resulting hydrogen bond has O3…O4 = 2.467(2) Å, with O3-H = 1.120(3) Å and H…O4 = 1.370(3) Å forming a hydrogen bond angle of 164.7(2)°. Anisotropic displacement parameters for the position define an ellipsoid with its long axis approximately parallel to *b*, that is, nearly parallel to the O3-O4 direction.

To test for proton position disorder in serandite, observed (F_{obs}), model (F_{calc}), and difference-Fourier (delF) maps of the neutron scattering density were calculated in the section containing the hydrogen bond. Figure 1a shows the observed scattering density (F_{obs}) in the plane of the hydrogen bond. Scattering density around H is negative (dashed lines) because H has a negative neutron scattering length whereas that for O is positive. The shape of the observed density peak between O3 and O4 indicates asymmetric broadening toward O4, similar in shape to the X-ray (electron density) difference-Fourier residuals in pectolite of Prewitt (1967), and Takéuchi and Kudoh (1977), and the X-ray results for serandite from this study. The asymmetry of the H position could not be adequately modeled by a symmetric ellipsoid as shown in the difference-Fourier map (F_{obs}-F_{calc}) in Figure 2a.

To improve the model, we constrained the H atom displacement parameter to be isotropic and re-calculated the difference-

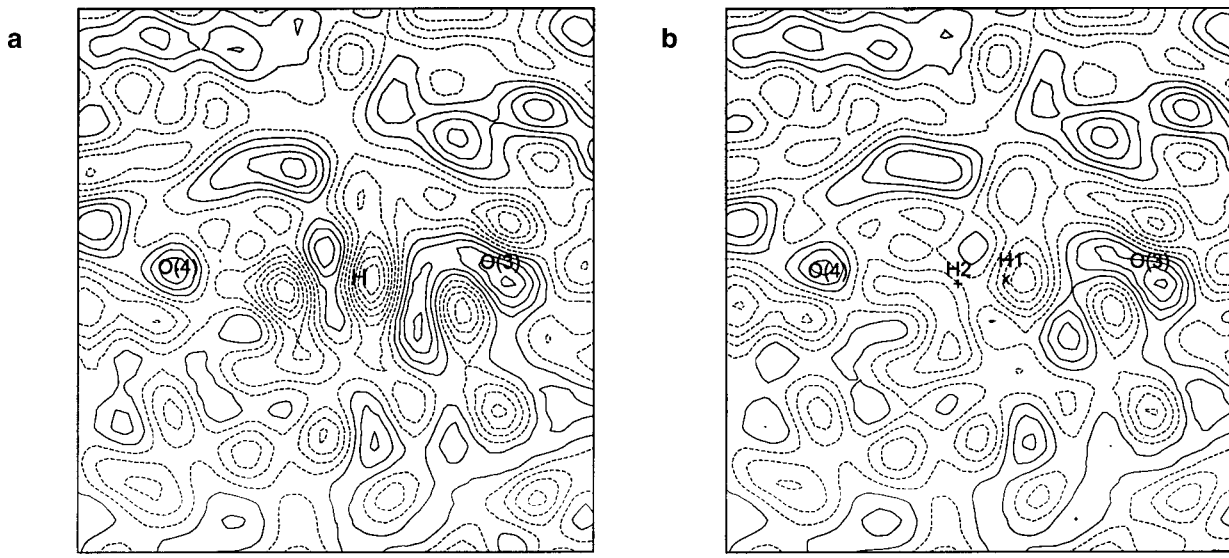

FIGURE 2. Maps of the difference-Fourier in serandite from neutron diffraction in the plane containing the hydrogen bond for (**a**) the one-proton model and (**b**) the two-proton model. Model positions are indicated by (H) for the one-proton model in (**a**) and by (x) and (+) for H1 and H2 in the two-proton model (**b**). The scale is 4 Å per side. The contour interval is 0.2, and ranges from –1.2 to 1.0 in (**a**) and –0.8 to 1.0 in (**b**). The zero and negative contours are dashed. Note that the two-proton model reduces the residual density between the oxygen positions O3 and O4.

Fourier map. A second H atom was placed at the point of maximum anomaly, and the relative occupancy parameters of the two, isotropic and fixed positions refined. The position close to O3 refines to about 86% and that nearest O4 to about 16%. The positional parameters of the two H-atoms in this "two-proton" model were then refined in separate cycles with fixed occupancy and isotropic displacement. Finally, displacement parameters were refined with H1 anisotropic and H2 isotropic. The positional parameters of H1 and H2 were again varied during the final cycles of least-squares, but the occupancy and displacement parameters were not. Model *R*-values are slightly reduced from the one-proton model with $R(F^2) = 0.100$ for all the data, and $R(F^2) = 0.098$ or $R(F) = 0.062$ for the set of data with $I > 3\sigma(I)$. Inspection of the difference-Fourier for the one- and two-proton models in Figure 2, reveals that residual scattering density between O3 and O4 is reduced (by about 30%) for the two-proton model. Atom positions from the final model of serandite from the neutron study are listed in Table 2, and displacement parameters are in Table 3. Hydrogen bond parameters for both configurations are summerized in Table 6.

DISCUSSION

Whereas it is possible to refine a single, ordered hydrogen position (H1) bonded to O3, the two-proton model is preferable for several reasons: (1) The two-proton position model yields slightly lower model $R(F^2)$ and $R(F)$ values. (2) The two-proton model reduces the residuals in the region of the difference-Fourier map between O3 and O4. (3) Both hydrogen bonds in the two-proton model are reasonable geometrically with respect to the O-H and H…O distances and hydrogen bond angles. Furthermore, a recalculation of the electrostatic potentials including the split H positions, give normal oxygen potentials at O3 and O4 of 29.0 and 27.6 V, respectively.

This study shows detectable site disorder of the H atom in serandite between two positions, one with 84%, and the other 16% of the scattering probability density. The first position (H1) is located 1.079(4) Å from O3 and 1.413(4) Å from O4. The second (H2) is located 1.075(9) Å from O4 and 1.402(9) Å from O3. The distance between the disordered H1 and H2 positions is 0.34(1) Å. The hydrogen bond angles involving the H1 and H2 positions are 164.0(3)° and 168(1.2)°, respectively. Therefore, we conclusively confirm by neutron diffraction in serandite an asymmetric double-minimum hydrogen bond.

These results also provide some insight into the unusual IR spectra of serandite and its isomorph, pectolite (Hammer et al. 1998). The relative strength of hydrogen bonds in crystals is related to the separation between the donor and acceptor oxygen, O_d-H…O_a. Emsley (1981) defines weak hydrogen bonds with O…O distances greater than 2.7 Å, strong hydrogen bonds between 2.5 and 2.7 Å, and those with O…O distances less than 2.5 Å as very strong. Compilations of O-H stretching frequency (ν) vs. O…O distance correlations (Novak 1974; Libowitzky 1999) provide a respective strength scale based on IR absorption bands. Using such correlations, O-H stretching frequencies above 3200 cm^{-1} are considered weak, those between 3200–1600 cm^{-1} are strong, and very broad bands below 1600 cm^{-1} are considered very strong. The correlation between

TABLE 6. Summary of the hydrogen bond parameters from neutron diffraction for the two (disordered) configurations in serandite

Parameter	Hydrogen bond	
	O3-H1…O4	O3…H2-O4
d(O· · ·O) (Å)	2.467(1)	2.467(1)
d(O-H) (Å)	1.078(3)	1.074(11)
d(H· · ·O) (Å)	1.413(3)	1.407(11)
bond angle	164.0(3)°	168(1)°

(ν)O-H and *d*(O…O), *d*(H…O), and perhaps *d*(H-O) provides the ability to infer hydrogen bond geometry and perhaps even proton positions from spectroscopic techniques. In addition, the application of frequency-distance correlations to spectroscopic measurements at high pressure may provide a tool for elucidation of hydrogen bond geometries as a function of pressure (Hofmeister et al. 1999).

The refined positions of O3 and O4 from our models result in a hydrogen bond distance O3…O4 = 2.464(1) Å and 2.467(1) Å in the X-ray and neutron models, respectively. This distance is slightly longer than 2.453(4) Å, reported for serandite by Takéuchi et al. (1976). Still, this hydrogen bond falls into the category of a very strong bond. In fact, Hammer et al. (1998) predicted an O3…O4 distance of 2.46–2.47 Å for serandite from their assignment of ν(O-H) = 1000 cm^{-1} and the frequency-distance correlation published by Novak (1974), in agreement to our result.

Knowledge of precise H positions from neutron experiments also allows for the correlation of *d*(O-H) or *d*(H…O) to ν(O-H). Libowitzky (1999) constructed a relation between frequency and *d*(H…O) in minerals from structures with well determined H positions that is modified in Figure 3. This figure includes data from silicates, hydroxides, carbonates, sulfates and phosphates, the new data for serandite is plotted as the filled circle with *d*(H1…O4) = 1.413(3) Å and *d*(H2…O3) = 1.407(11) Å. These data, given 1000 cm^{-1} ν(O-H) determined by Hammer et al (1998), fall exactly on the extrapolation (dashed line) of the relation determined by Libowitzky (1999) (solid line) from the 43 data with ν(O-H) > 2500 cm^{-1} given by $\nu = 3632 - 1.79\ 10^6 \exp(-d/0.2146)$. In this correlation, the region of very strong hydrogen bonds is occupied

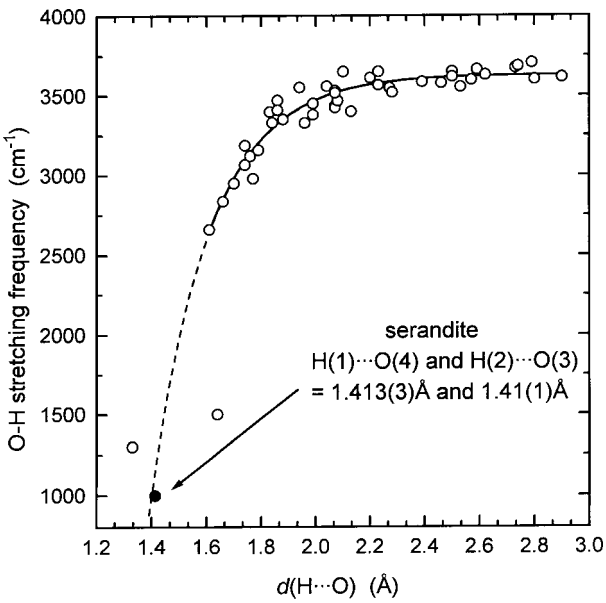

FIGURE 3. Plot of O-H stretching frequency ν (cm^{-1}) vs. the distance *d*(H…O) (Å) [modified after Libowitzky (1999)]. This correlation diagram includes 46 data pairs from a variety of naturally occurring minerals with well determined H positions. The solid line regression is fit to the 43 data with stretching frequencies greater than 2500 cm^{-1} whereas the dashed part is only an extrapolation of that function.

by two other data which do not fall on the extrapolation. Namely, Trona, $Na_3(CO_3HCO_3)\cdot 2H_2O$, at about 1300 cm^{-1} and shorter H…O distance and mozartite, $CaMnOSiO_3(OH)$, at about 1500 cm^{-1} and a longer H…O distance.

In theory, the fundamental stretching ν(O-H) should be nearly proportional to the O-H distance for weak hydrogen bonds. Novak (1974) reports a correlation of O-H distance with ν(O-H) for twenty-one compounds and minerals for which the proton position is reasonably well determined. The data set of Novak (1974) shows a linear (negative) relationship between ν(O-H) and *d*(O-H) given by $\Delta\nu/\nu_0 = 3.6\ \Delta\ d$(O-H) with the exception of three data pairs that fall to the left of this trend (O-H distance too short) and one which falls to the right (O-H distance too long). Novak (1974) points out that these points which vary significantly from the trend correspond to compounds for which there is a reported symmetric double-minimum. Using a value of ν(O-H) of about 1000 cm^{-1} for serandite (Hammer et al. 1998) and the *d*(O-H) distances for the H1 and H2 positions from this study we find that serandite also plots well below the trend of Novak (1974). So the O-H distances and ν(O-H) stretching frequencies in serandite are consistent with previous observations of hydrogen bonds with double-minima.

In general, Si-OH bonds tend to be longer than their respectively coordinated Si-O bonds. Nyfeler and Armbruster (1998) report an average Si-OH bond length of 1.643 Å, compared to 1.626 Å for the average Si-O bond length commonly cited for the silicate tetrahedra of rock-forming minerals (Gibbs 1982). From Table 4, the silanol group Si1-O3H1 bond length in serandite is 1.628(1) Å. Although this is rather short for a silanol group, it is 0.027(1) Å longer than Si1-O5, 0.014(1) Å longer than Si1-O(9), but 0.020(1) Å shorter than Si1-O(7). In the partially hydrated Si2 tetrahedron, the silanol group Si2-O4H2 is the shortest Si-O bond. The average Si-O bond length (including Si-OH) of the hydrated silicate tetrahedron containing Si1 is 1.623 Å, and statistically identical to the average Si-O bond distance of the Si2 tetrahedra, but significantly shorter than the average Si-O of the unhydrated Si3 tetrahedron (=1.634 Å). In fact, this not so unusual considering that Nyfeler and Armbruster (1998) also observe that the average *d*(Si-OH) tends to decrease as the number of bridging oxygen atoms (Si-O-Si) decreases in the hydrated SiO_4 tetrahedron so that <Si-O> can even exceed *d*(Si-OH) in silicate tetrahedra with three bridging oxygen atoms.

Structural effects of protonation of the non-silicate oxygen may also be discussed in terms of polyhedral volume and distortion parameters (Table 4). Whereas the hydrated Si1 and Si2 tetrahedra have identical volumes of about 2.17–2.18 $Å^3$, the unhydrated Si3 tetrahedron joining the two is considerably larger with a volume of about 2.22 $Å^3$. The deviation of O-Si-O angles from an ideal tetrahedron (109.47°) can be estimated by the tetrahedral angle variance, $\sigma^2_{\theta(tet)}$, in Table 5. The dominantly hydrated Si1 tetrahedron shows the most variation from ideality, with an angle variance of about 25.1. The value of $\sigma^2_{\theta(tet)}$ for the Si2 and Si3 tetrahedron are 20.1 and 21.0, respectively. It is difficult however to determine exactly what effects protonation of the silicate oxygen have on the tetrahedra because the geometry of the chain is also constrained by the ad-

joined edge-sharing chain of Mn-octahedra.

In conclusion, the hydrogen bond in serandite is rather unusual for silicate minerals. Silicate tetrahedra are, in general, rigid structural units, so it is likely that the silicate chain geometry exerts a stronger control on the O…O distance than does the hydrogen bonding. The unique geometry of the 3-repeat tetrahedral chain allows the very short hydrogen bond in serandite to distribute extra charge over two non-bridging silicate-oxygen atoms. In this way, the short O…O distance actually facilitates protonation of a silicate oxygen without the overbonding that would usually result from protonation of an oxygen that is also bonded to silicon. Double-well potentials in very short hydrogen bonds most likely result from the contribution of the nearby supplementary attractive potential from the proton-acceptor oxygen, in this case, O4. The calculated electrostatic environment around O3 and O4 indicate that the proton should favor O3 over O4. Therefore the relative proton occupation refined in our model, ~84% O3-H…O4 and ~16% O3…H-O4, may be purely statistical in nature—reflecting the relative depth of the two energy minima.

ACKNOWLEDGMENTS

This research was supported by the National Science Foundation, grant EAR97-25672 to J.R.S. Support for the neutron scattering experiment was provided by the Los Alamos National Laboratory, operated by the University of California under grant W-7405-ENG-36 from the U.S. Department of Energy. The authors wish to thank Allen Larson for his assistance with the data collection at the Los Alamos Neutron Scattering Center. We are also grateful for the constructive reviews of J. Fitzpatrick, H. Keppler, and E. Libowitzky.

REFERENCES CITED

Beran, A., Giester, G., and Libowitzky, E. (1997) The hydrogen bond system in natrochalcite-type compounds—an FTIR spectroscopic study of the $H_3O_2^-$ unit. Mineralogy and Petrology, 61, 223–235.

Bergerhoff, G., Hundt, R., Sievers, R., and Brown, I.D. (1983) ICSD, Inorganic Crystal Structure Database. Journal of Chemical Information and Computer Sciences, 23, 66–69.

Becker, P.J. and Coppens, P. (1974) Extinction within the limit of validity of the Darwin Transfer Equations I: General formalisms for primary and secondary extinction and their application to spherical crystals. Acta Crystallographica, A30, 129–147.

Borkowski, C.J. and Kopp, M.J. (1978) Recent improvements to R-C line encoded position-sensitive proportional counters. Journal of Applied Crystallography, 11, 430–434.

Buerger, M.J. (1956) The determination of the crystal structure of pectolite, $Ca_2NaHSi_3O_9$. Zeitschrift für Kristallographie, 108, 248–262.

Emsley, J. (1981) Very strong hydrogen bonding. Chemical Society Reviews, 9, 91–124.

Gibbs, G.V. (1982) Molecules as models for bonding in silicates. American Mineralogist, 67, 421–450.

Finney J.L. (1995) The complementary use of X-ray and neutron diffraction in the study of crystals. Acta Crystallographica, B51, 447–467.

Hammer, V.M.F., Libowitzky, E., and Rossman, G.R. (1998) Single-crystal IR spectroscopy of very strong hydrogen bonds in pectolite, $NaCa_2[Si_3O_8(OH)]$, and serandite, $NaMn_2[Si_3O_8(OH)]$. American Mineralogist, 83, 569–576.

Hofmeister, A.M., Cynn, H., Burnley, P.C., and Meade, C. (1999) Vibrational spectra of dense, hydrous magnesium silicates at high pressure: Importance of the hydrogen bond angle. American Mineralogist, 84, 454–464.

Kuroda, Y., Suzuoki, T., and Matsuo, S. (1979) The lowest dD value found in a hydrous silicate, pectolite. Nature, 279, 227–228.

Libowitzky, E. (1999) Correlation of O-H stretching frequencies and O-H···O hydrogen bond lengths in minerals. Monatshefte fur Chemie, 130, 1047–1059.

Larson, A.C. and Von Dreele, R.B. (1994) Los Alamos National Laboratory, General Structure Analysis System (GSAS). LA-UR 86-748, Los Alamos, New Mexico.

Lutz, H.D. (1995) Hydroxide ions in condensed materials—correlation of spectroscopic and structural data. Structure and Bonding, 82, 85–103.

Mikenda, W. (1986) Stretching frequency versus bond distance correlation of O-D(H)···Y (Y = N, O, S, Se, Cl, Br, I) hydrogen bonds in solid hydrates. Journal of Molecular Structure, 147, 1–15.

Nakamoto, K., Margoshes, M., and Rundle R.E. (1955) Stretching frequencies as a function of distance in hydrogen bonds. Journal of the American Chemical Society, 77, 6480–6488.

Novak, A. (1974) Hydrogen bonding in solids. Correlation of spectroscopic and crystallographic data. Structure and Bonding, 18, 177–216.

Nyfeler, D. and Armbruster, T. (1998) Silanol groups in minerals and inorganic compounds. American Mineralogist, 83, 119–125.

Ohashi, Y. (1976) Hydrous pyroxenoids: Stepwise substitution of Mn and Ca in the pectolite- schizolite-serandite series, $(Ca,Mn)_2NaHSi_3O_9$. Geological Society of America, Abstracts with Program, 8, 1034.

Ohashi, Y. and Finger, L.W. (1978) The role of octahedral cations in pyroxenoid crystal chemistry. I. Bustamite, wollastonite, and the pectolite-schizolite-serandite series. American Mineralogist, 63, 274–288.

Pauling, L. (1980) The nature of silicon-oxygen bonds. American Mineralogist, 65, 321–323.

Prewitt, C.T. (1967) Refinement of the structure of pectolite, $Ca_2NaHSi_3O_9$. Zeitschrift für Kristallographie, 125, 298–316.

Prewitt, C.T. and Buerger, M.J. (1963) Comparison of the crystal structures of wollastonite and pectolite. Mineralogical Society of America, Special Paper, 1, 293–302.

Robinson, K., Gibbs, G.V., and Ribbe, P.H. (1971) Quadratic elongation: A quantitative measure of distortion in coordination polyhedra. Science, 172, 567–570.

Sheldrick, G. (1990) SHELXTL-PC (Release 4.1), 296 p. Siemens Analytical X-ray Instruments, Inc., Madison, Wisconsin.

Smyth, J.R. (1987) β-Mg_2SiO_4: A potential host for water in the mantle? American Mineralogist, 72, 1051–1055.

———(1989) Electrostatic characterization of oxygen sites in minerals. Geochemica et Cosmochimica Acta, 53, 1101–1110.

Smyth, J.R. and Clayton, R.N. (1988) Correlation of oxygen isotope fractionation and electrostatic site potentials in silicates. Transactions, American Geophysical Union, Program with Abstracts, 69, 1514.

Takéuchi, Y. and Kudoh, Y. (1977) Hydrogen bonding and cation ordering in Magnet Cove pectolite. Zeitschrift für Kristallographie, 146, 281–292.

Takéuchi, Y., Kudoh, Y., and Yamanaka, T. (1976) Crystal chemistry of the serandite pectolite series and related minerals. American Mineralogist, 61, 229–237.

MANUSCRIPT RECEIVED JUNE 15, 1999
MANUSCRIPT ACCEPTED DECEMBER 1, 1999
PAPER HANDLED BY BRYAN CHAKOUMAKOS